The Plant Journal (2006) **48**, 367–379 doi: 10.1111/j.1365-313X.2006.02883.x

Identification of plant cytoskeleton-interacting proteins by screening for actin stress fiber association in mammalian fibroblasts

Mohamad Abu-Abied[1], Lior Golomb[1], Eduard Belausov[1], Shanjin Huang[2], Benjamin Geiger[3], Zvi Kam[3], Christopher J. Staiger[2] and Einat Sadot[1,*]

[1]*The Institute of Plant Sciences, The Volcani Center, Bet-Dagan 50250 Israel,*

[2]*Department of Biological Sciences and the Bindley Bioscience Center, Purdue University, West Lafayette, IN 47907-2064, USA, and*

[3]*The Department of Cell Molecular Biology, The Weizmann Institute of Science, Rehovot 76100, Israel*

Received 16 April 2006; revised 25 June 2006; accepted 3 July 2006.
*For correspondence (fax 972 3 966 9583; e-mail vhesadot@agri.gov.il).

Summary

Taking advantage of the high conservation of the cytoskeleton building blocks actin and tubulin between plant and animal kingdoms, we developed a functional genomic screen for the isolation of new plant cytoskeleton-binding proteins that uses a mammalian cell expression system. A yellow fluorescent protein (YFP)-fusion cDNA library from Arabidopsis was inserted into rat fibroblasts and screened for fluorescent chimeras localizing to cytoskeletal structures. The high-throughput screen was performed by an automated microscope. An initial set of candidate genes identified in the screen was isolated, sequenced, the full-length cDNAs were synthesized by RT-PCR and tested by biochemical approaches to verify the ability of the genes to bind actin directly. Alternatively, indirect binding via interaction with other actin-binding proteins was studied. The full-length cDNAs were transferred back to plants as YFP chimeras behind the CAMV-35S promoter. We give here two examples of new plant cytoskeletal proteins identified in the pilot screen. ERD10, a member of the dehydrin family of proteins, was localized to actin stress fibers in rat fibroblasts. Its direct binding to actin filaments was confirmed by several biochemical approaches. Touch-induced calmodulin-like protein, TCH2, was also localized to actin stress fibers in fibroblasts, but was unable to bind actin filaments directly *in vitro*. Nevertheless, it did bind to the IQ domains of Arabidopsis myosin VIII in a calcium-dependent manner. Further evidence for a cytoskeletal function of ERD10 was obtained *in planta*; GFP-ERD10 was able to protect the actin cytoskeleton from latrunculin-mediated disruption in *Nicotiana benthamiana* leaves.

Keywords: cytoskeleton, yellow fluorescent protein (YFP), cDNA library, high-throughput, screen.

Introduction

The cytoskeleton evolved before plants diverged from animals, and the main features of the cytoskeleton have been conserved in both; however, specialized cytoskeletal structures and specific cytoskeleton-mediated mechanisms evolved separately. Indeed, there is recent evidence for a pro-karyotic origin of microtubule- and actin-based cell skeletons (reviewed in Moller-Jensen and Lowe (2005). For several cytoskeletal proteins, the similarity in the amino acid sequence is well conserved between the two kingdoms. For example, the amino acid sequence similarity between actin and tubulin from Arabidopsis and human is 80–90% (Meagher and Williamson, 1994). In addition, some of the actin-associated proteins are relatively well-conserved between plants and animals, these include profilin (30% identity in amino acid sequence and the three-dimensional structure is well conserved; Thorn *et al.*, 1997), cofilin or actin depolymerizing factor (ADF; 30% identity; Carlier *et al.*, 1997; Dong *et al.*, 2001), unconventional myosins (80% identity in the S1 domain; Kinkema and Schiefelbein, 1994), fimbrin (40% overall similarity and up to 74% similarity in the actin-binding domain; McCurdy and Kim, 1998), villin (80% similarity in the G1 domain; Klahre *et al.*, 2000; Vidali *et al.*, 1999)

and ARP2 and ARP3 from Arabidopsis have 62% and 60% sequence identity to human Arp2 and Arp3, respectively (McKinney *et al.*, 2002). Other components of the ARP2/3 complex, as well as ARP2/3 activators and WAVE complex subunits, were recently characterized in plants and show high homology to their mammalian counterparts (Mathur, 2005; Szymanski, 2005). Moreover, some plant cytoskeletal binding proteins recognize either animal actin filaments or microtubules; for example, Arabidopsis VILLIN-GFP fusions decorate actin filament stress fibers and membrane protrusions in mammalian Vero cells (Klahre *et al.*, 2000), MAP65 from carrot co-polymerizes with porcine brain microtubules (Chan *et al.*, 1999), myosin from Chara translocates muscle F-actin in an *in vitro* motility assay at a similar velocity (60 μm sec^{-1}) as cytoplasmic streaming in this alga (Higashi-Fujime *et al.*, 1995) and birch pollen profilin binds to human VASP directly and stabilizes microfilaments in animal cells (Reinhard *et al.*, 1995; Rothkegel *et al.*, 1996). Despite the similar sequence and structure of the cytoskeleton building blocks, there are still missing protein mediators for known plant cytoskeletal functions; for example, cortical microtubules are connected to the plasma membrane as shown by electron microscopy (Gunning and Hardham, 1982; Vesk *et al.*, 1996) by unidentified protein links. Although a great deal of progress has been made recently regarding signaling to the cytoskeleton (Fu *et al.*, 2005; Gu *et al.*, 2005; Huang *et al.*, 2006), many of the proteins delivering either the stimulus or the signal are still missing (Deeks *et al.*, 2002). Extensive searches of the completed Arabidopsis genome database (AGI, 2000) reveal the presence and elaboration of several classes of actin and actin-binding proteins (Meagher *et al.*, 1999). However, many of the >70 classes of eukaryotic actin-binding proteins (Kreis and Vale, 1999; Pollard, 2001) are apparently either absent or poorly conserved in Arabidopsis (Assaad, 2001; Drøbak *et al.*, 2004; Hussey *et al.*, 2002; Staiger and Hussey, 2004), including spectrin, α-actinin, filamin, thymosin β4 and others. Plant analogues of these proteins may exist but they may share tertiary structure rather than primary sequence conservation (Deeks and Hussey, 2003). This strongly suggests that further screens should be based on function rather than on bio-informatics or on cross-reaction with antibodies.

Thus, based on the high conservation of the cytoskeletal building blocks (actin and tubulin) between the animal and plant kingdoms, and on the clear and easy identification of cytoskeletal localization with fluorescence microcopy, we developed a method for screening an Arabidopsis cDNA library fused to yellow fluorescent protein (YFP) in rat fibroblasts. As proof of concept, a small portion of the library was screened, and several new cytoskeletal-associated proteins were discovered. We give here two examples of plant genes, ERD10 and touch-induced calmodulin-like protein, TCH2 that were localized to actin stress fibers in Rat embryo fibroblast cells (Ref52)and give biochemical evidence that they bind actin either directly or indirectly *in vitro*. Furthermore, overexpression of ERD10 in *Nicotiana benthamiana* cells conferred resistance to actin filaments against the depolymerizing effects of latrunculin B. Collectively, these results demonstrate the power of this heterologous screening system for the identification of new cytoskeletal proteins from plants.

Results

The library

A library of partial Arabidopsis cDNAs fused to Venus YFP was constructed as described in Experimental procedures (Figure 1). In order to verify the quality of the library 30 random clones were sequenced. It was found that among the 30 clones, none were an empty vector and all clones were oriented 5′ → 3′ with insert sizes ranging from 50 to 600 nucleotides. Furthermore, no clones corresponding to ribosomal RNA were found. Transforming the library into XL1 Blue *Escherichia coli* competent cells was highly efficient resulting in more than 100 000 colonies, ~60 000 of which were collected. In a control experiment, DNA made from a pool of 2500 clones and a mixture of the empty vectors was transfected into 293T cells. It was found that although the transfection of the library resulted in many fluorescent cells (Figure 2 c,d), the empty vectors gave only background fluorescence (Figure 2 a,b), proving that each fluorescent clone observed in the screen contained an Arabidopsis cDNA insert in frame with YFP.

The screen

Ref52 cells were plated in 384-well plates and infected. After 48 h when expression had peaked, the culture was already

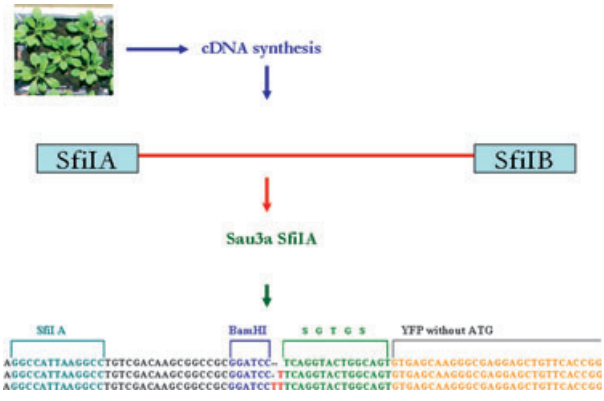

Figure 1. Schematic representation of the strategy for constructing the YFP-fusion cDNA library. cDNA was synthesized, and flanked by two restriction sites of *Sfi*I A and B. It was then digested by *Sfi*I followed by partial digestion with *Sau*3A and ligated into *Sfi*IA–*Bam*HI sites fused to YFP in three reading frames.

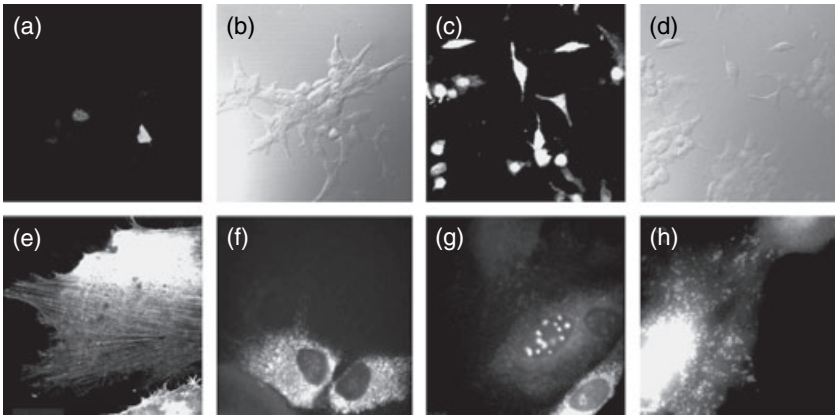

Figure 2. Mammalian cells transfected with the library.
(a, b) A mixture of the empty vectors and (c, d) a sample of the library, were transfected into 293T cells and examined by fluorescence microscopy. It is demonstrated that the empty vectors yielded only background fluorescence, whereas the library contained many clones inserted in frame with the 'ATG-less' YFP and activated its expression.
(e-h) Ref52 rat fibroblasts, expressing different clones from the library. Different examples show localization to actin stress fibers (e), the perinuclear region (f), punctuate structures in the nucleus (g) and cytoplasmic structures (h).

confluent and covered the whole well. At this stage the cells were fixed. For the automatic high-resolution high-throughput screen we used an ×60/0.9 Numerical Aperture objective yielding images with field dimensions of 111 × 111 μm. The size of a Ref52 cell is approximately 60 × 60 μm. Thus it was possible to allow 20-μm gaps between the acquired fields and still sample all cells in each well. In addition, a rim of -four-fields thick around the well periphery was not acquired because of poor optical conditions near the well edges. Altogether, the screen included 256 images from each well (Figure S1). The time for each image acquisition (auto focusing, exposure of 1 sec and the movement of the stage to the next field) was 2 sec. Thus, a full-plate screen required 55 h (or 2.25 days). The computer memory required for storing this information was approximately 80 Gb. The infection efficiency was calibrated to 30–60% to ensure that no more than between one and three retrovirus integrations occurred, which might result in the masking of a specific localized clone by a diffuse cytoplasmic localized one. It was found in a pilot screen of 2500 clones that the number of fluorescent cells matched the expected efficiency of infection well. Specifically, the 10–20% fluorescent cells observed (with fluorescence levels clearly above background) indicated a 30–60% efficiency, because only one third of the clones are in frame and fluorescent. A majority of the fluorescent cells exhibited diffuse cytoplasmic fluorescence. About 5% displayed staining patterns with sub-cellular localization such as to the perinuclear region, the nucleus or cytoplasmic structures (Figure 2 f–h), and about 1% were localized to cytoskeletal structures such as actin stress fibers (Figure 2e).

The isolation and characterization of ERD10 and TCH2 as new plant cytoskeleton-associated proteins

Some of the clones showing cytoskeletal localization in the pilot screen were isolated and sequenced (Figure S2). Several clones contained an in-frame fusion with YFP, whereas others contained fragments from more than one gene fused in frame to YFP, and a few clones were fused to YFP in a different open reading frame than the annotated gene, creating peptides with the ability to bind actin stress fibers. At present we consider the latter to be the background of the system. In the future when completing a comprehensive screen we will use bioinformatics to study the presence of relevant amino acid key words in their sequence (Wise, 2003). In the small-scale pilot screen presented here we did not isolate any known actin-binding proteins; however, we fused the actin-binding domain 2 (ABD2) from Arabidopsis FIMBRIN1 to YFP in the mammalian expression vector and expressed it in Ref52 cells as a positive control (Figure 3). We chose two of the most promising genes isolated in the pilot screen for further study and to prove the concept of this unique method. The two clones chosen, both of which gave prominent labeling of actin stress fibers in Ref52 cells (Figure 3), contained fragments belonging to ERD10, a member of the dehydrin family (Kiyosue *et al.*, 1994), and TCH2 (Braam and Davis, 1990). It is noteworthy that a second dehydrin family member, COR47, was also recovered from the pilot screen (Figure S2). The full-length cDNAs were isolated, fused to YFP and re-transfected into Ref52 cells. Fixation was carried out in the presence of 0.5% Triton X-100 in order to remove soluble cytoplasmic proteins and double immuno-staining for actin and vinculin was performed. As shown in Figure 3, the stress fibers in Ref52 cells are decorated with the ERD10- and TCH2-YFP chimeras, as well as a known plant actin-binding protein, AtFIMBRIN1 actin-binding domain 2 (FABD2) as a positive control. The structures labeled with the newly isolated genes, ERD10 and TCH2, were also stained with fluorescent phalloidin (an F-actin binding reagent) and their ends were marked by vinculin labeling (a marker for focal contacts). This proves that the filamentous structures labeled by ERD10-YFP and TCH2-YFP are genuine actin stress fibers (Figure 3).

To examine whether the decoration of stress fibers in Ref52 cells results from the ability of these putative actin-interacting proteins to bind actin filaments directly, we expressed recombinant proteins as fusions with GST in

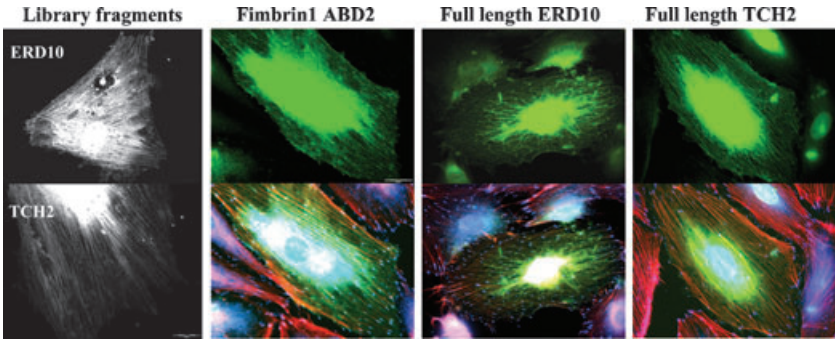

Figure 3. The ERD10 and TCH2 original fragments from the library and full-length cDNAs fused to YFP were transfected into Ref52 fibroblasts.
On the left, the two original fragments isolated from the library show prominent labeling of actin stress fibers in Ref52 cells. The subcellular distribution of the full-length cDNAs was compared with Arabidopsis FIMBRIN1 ABD2 in Ref52 cells. The top image of each pair (columns) shows the YFP fluorescence (green) from a representative cell. Double immunostaining of the cells expressing the plant fluorescent chimeras was performed, and overlay images are given in the bottom panel for each pair. Actin was labeled with coumarine-phalloidin and digitally colored red, and vinculin was stained with anti-vinculin antibody and a Cy3-conjugated secondary antibody and digitally colored blue. It is shown that similar to Fimbrin1 ABD2, ERD10 and TCH2 are co-localized with actin stress fibers in Ref52 cells. Scale bar = 20 μm.

bacterial cells. Fusion proteins were isolated by affinity chromatography, the GST-tag removed by thrombin cleavage and the resulting purified recombinant protein tested for binding to actin filaments prepared from muscle α-actin isoform. Initially, high-speed co-sedimentation assays were performed to detect interactions between side-binding proteins and pre-formed actin filaments (Huang *et al.*, 2004; Kovar *et al.*, 2000; Michelot *et al.*, 2005). ERD10, but not TCH2, demonstrated binding to actin filaments in a dose-dependent manner (data not shown). Compared with Arabidopsis FIMBRIN1 (AtFIM1; K_d for actin filaments ~0.5 μM; Kovar *et al.*, 2000), the binding of ERD10 appeared to be somewhat weaker. Unfortunately, a substantial quantity of ERD10 also sedimented in the absence of actin filaments, making an accurate determination of K_d impossible.

To confirm the binding of ERD10 to actin filaments, several either kinetic or steady state assays for actin polymerization were performed using pyrene-labeled actin. At steady state, the actin-monomer binding protein profilin increased the critical concentration (C_c) for actin filament assembly by sequestering actin subunits and preventing their polymerization (Figure 4a). ERD10 had the opposite effect on actin polymerization, markedly lowering the C_c value at equilibrium (Figure 4a), and this is consistent with the stabilization of actin filaments. When actin polymerization from monomers was monitored as a function of time, a typical curve for assembly showed a lag period for actin filament nucleation, a period of rapid growth and ultimately a plateau of polymer formation (Figure 4b). ERD10 inhibited actin polymerization in a dose-dependent manner, extending the period required for nucleation and reducing the rate of polymerization (Figure 4b). The filament side-binding and cross-linking protein AtFIM1 had similar effects in this assay (data not shown). Also, like AtFIM1 (Figure 4d), ERD10 inhibited actin filament depolymerization following dilution (Figure 4c). Increasing quantities of ERD10 reduced the rate and extent of actin filament disassembly in a dose-dependent manner, but was not quite as potent as AtFIM1 under the identical conditions. The collective results strongly support the notion that ERD10 is capable of binding to either the side or the ends of actin filaments *in vitro* and alters the dynamics of actin.

As for TCH2, which did not bind and co-sediment with actin filaments *in vitro*, it was still plausible that it bound Ref52 actin stress fibers indirectly by associating with another actin-binding protein. Calmodulin and calmodulin-like proteins can be myosin light chains through binding to the IQ domain(s) on the heavy chains of both conventional and unconventional myosins (reviewed in Bahler and Rhoads, 2002; Cyert, 2001; McCormack *et al.*, 2005). Therefore, we considered the possibility that overexpressed plant TCH2 was recognizing and binding the IQ domain of non-muscle rat myosin II, and thereby associating with the actin stress fibers of Ref52 cells. In order to address the question of whether TCH2 has the potential to be a plant myosin light chain, a fragment of cDNA corresponding to the four IQ domains of myosin VIII from Arabidopsis (ATM1) was fused to GST. It was found that TCH2-YFP was pulled down by GST-IQ in a calcium-dependent manner (Figure 5a). In order to obtain more information about the specificity of the interaction between TCH2 and the IQ domain of ATM1, we characterized another isoform of TCH. TCH1 is a touch-induced calmodulin that was originally isolated in the same screen together with TCH2 (Braam and Davis, 1990). We cloned the TCH1 cDNA and expressed it as a YFP fusion protein. As myosin light chains are generally either calmodulins or calmodulin-like proteins, it was important to determine whether the IQ domain of myosin VIII binds either generally or specifically to these proteins. In contrast to TCH2, TCH1 was unable to bind to the ATM1 IQ domain in a pull-down assay (Figure 5b), which reinforces the specificity of the TCH2/IQ interaction.

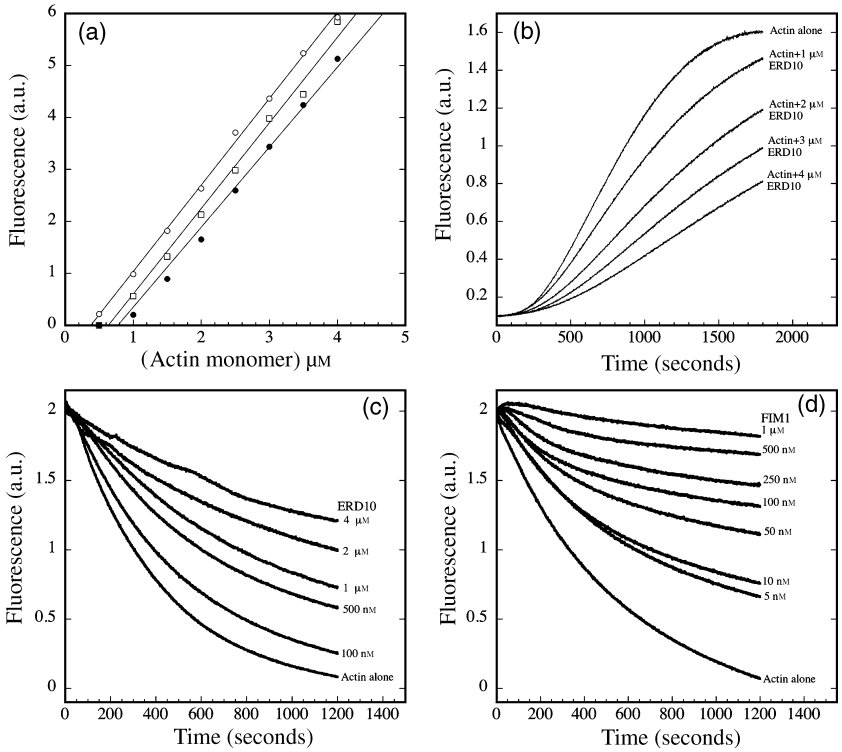

Figure 4. ERD10 affects actin assembly and disassembly directly.
(a) Determination of the critical concentration (C_c) for actin assembly in the absence and presence of either ERD10 or human profilin, HPRO1. Increasing concentrations of actin were incubated in either the absence (open squares) or the presence of 2 μM ERD10 (open circles) or 1 μM HPRO1 (closed cirlces) and allowed to polymerize for 16 h at room temperature. To cap filament barbed ends, a 1:200 ratio of human plasma gelsolin : actin was included in all reactions. Fluorescence emission from pyrene-actin assembly was recorded with the fluorimeter. The C_c values (*x*-axis intercept of each regression line) for this representative experiment were 0.63 μM for actin alone, 0.38 μM for ERD10 and 0.77 μM for HPRO1. a.u., arbitrary units.
(b) ERD10 inhibits actin polymerization. ERD10 at various concentrations was incubated for 5 min with 2 μM actin (5% pyrene-labeled) before polymerization. Pyrene fluorescence is plotted versus time after the addition of KMEI buffer (described in Experimental procedures) to initiate polymerization. ERD10 extended the lag period (or nucleation phase) and reduced the initial rate of actin assembly in a dose-dependent manner. a.u., arbitrary units.
(c, d) ERD10 and AtFIM1 stabilize actin filaments and inhibit depolymerization. Actin in polymeric form (5 μM; 100% pyrene labeled) was incubated with various concentrations of either ERD10 (c) or AtFIM1 (d) for 5 min before dilution of the solution 25-fold. Concentrations given are for each protein after dilution. Both actin binding proteins reduced the rate and extent of actin filament depolymerization in a dose-dependent fashion. However, FIM1 appeared to be more potent, almost completely preventing depolymerization at 1 μM, when compared with ERD10 at the same concentration.

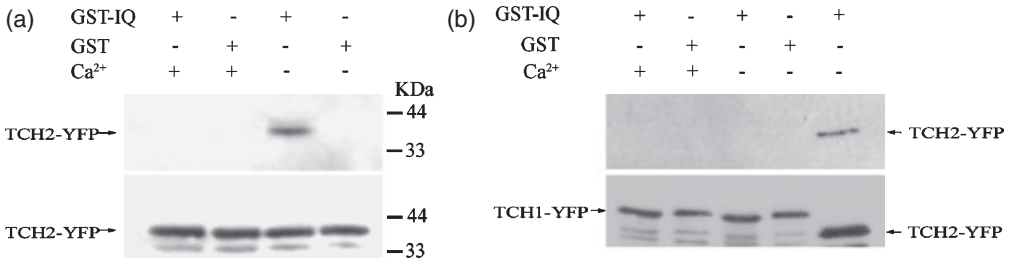

Figure 5. Pull down assay of GST-IQ and either YFP-TCH2 or YFP-TCH1. The 4XIQ domain from ATM1 (Arabidopsis myosin VIII) was fused to GST and collected from bacterial extract using glutathione agarose beads. These beads were incubated with extracts from 293T cells expressing either TCH2-YFP or TCH1-YFP in either the presence or the absence of free Ca^{2+}. Beads were precipitated, washed and boiled in sample buffer and bound proteins were separated on SDS-PAGE and detected with anti-GFP antibody.
Upper panels, pull-down assay; lower panels, total 293T cell extracts.
(a) TCH2 fused to YFP.
(b) TCH1 fused to YFP. It is shown that although TCH2 binds the 4XIQ domain of ATM1 in a calcium-sensitive manner no such binding was observed for TCH1, suggesting specificity of the interaction between TCH2 and the ATM1 4XIQ domain.

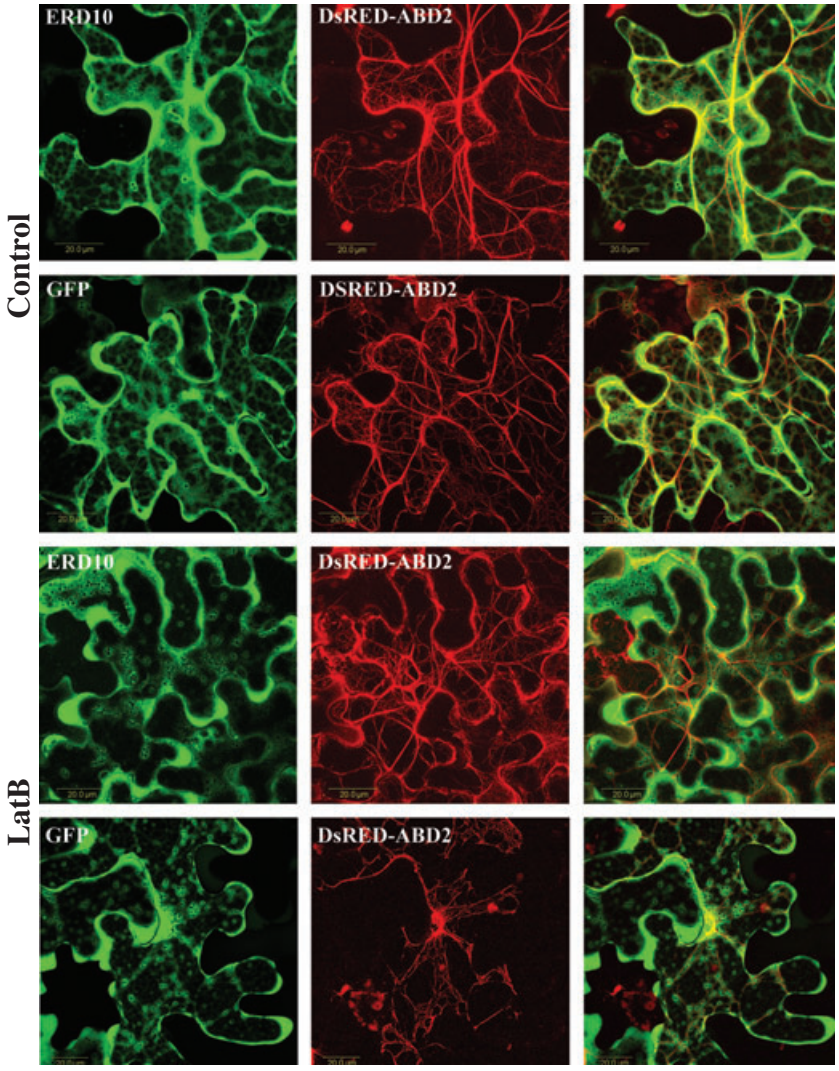

Figure 6. ERD10 is able to protect the actin cytoskeleton from LatB-mediated disruption in *N. benthamiana* leaves.
A chimera of GFP-ERD10, or GFP alone, was infiltrated into *N. benthamiana* leaves together with DsRED-ABD2. After 48 h leaf disks were treated with 25 μM LatB for 5 h and inspected by the confocal microscope. Images show fluorescence caused by ERD10-GFP or GFP alone in green (left-hand panels), the actin cytoskeleton decorated with DsRED-ABD2 in red (middle panels), and an overlay of both signals (right-hand panels). It is shown that in the presence of ERD10 the actin cytoskeleton was barely affected by the drug, whereas in the presence of GFP alone significant disruption was observed. Scale bar = 20 μm.

Co-expressing ERD10 as a GFP chimera with DsRED-ABD2

In order to learn more about the possible interaction and effect of ERD10 on the actin cytoskeleton *in planta*, we labeled actin and ERD10 with two different fluorescent proteins. The fluorescent chimeras of GFP-ERD10 and DsRED-ABD2 (the second actin binding domain from Arabidopsis fimbrin 1 that binds to actin filaments (Voigt *et al.*, 2005), were transiently expressed in *N. benthamiana* leaves using Agrobacterium infiltration (Figure 6). As a control, DsRED-ABD2 was co-expressed with GFP alone. The subcellular localization of ERD10 was mainly cytoplasmic, perhaps because of overexpression. Two days after infiltration, leaf disks were treated with Latrunculin B (LatB) for 5 h and then inspected with the confocal microscope. As shown in Figure 6, in the presence of GFP alone, actin filaments were severely disrupted by LatB. However, in the presence of ERD10 the actin cytoskeleton was protected from LatB-mediated disruption, which is consistent with our *in-vitro* data. Quantitative analysis of LatB-mediated disruption of actin in the presence of either GFP-ERD10 or GFP alone was performed with the Fiberscore image analysis software (Lichtenstein *et al.*, 2003). Ten independent microscopic fields from different leaves were examined in three different experiments. In each image, the signal coming from near the cell wall was deleted in order to ensure that the computer reads only genuine actin filaments (Figure 7), and then the image was subjected to Fiberscore analysis. As shown in Figure 7, each actin filament and actin cable in the original image was interpreted by the computer as a cytoskeletal element and was given a color according to its direction (which is irrelevant in this case). The summary of such analysis showed that, in the presence of ERD10, more than 70% of the filament-associated intensity and 70% of the total area of filamentous structures remained after LatB treatment, whereas in the presence of GFP alone <40% of the

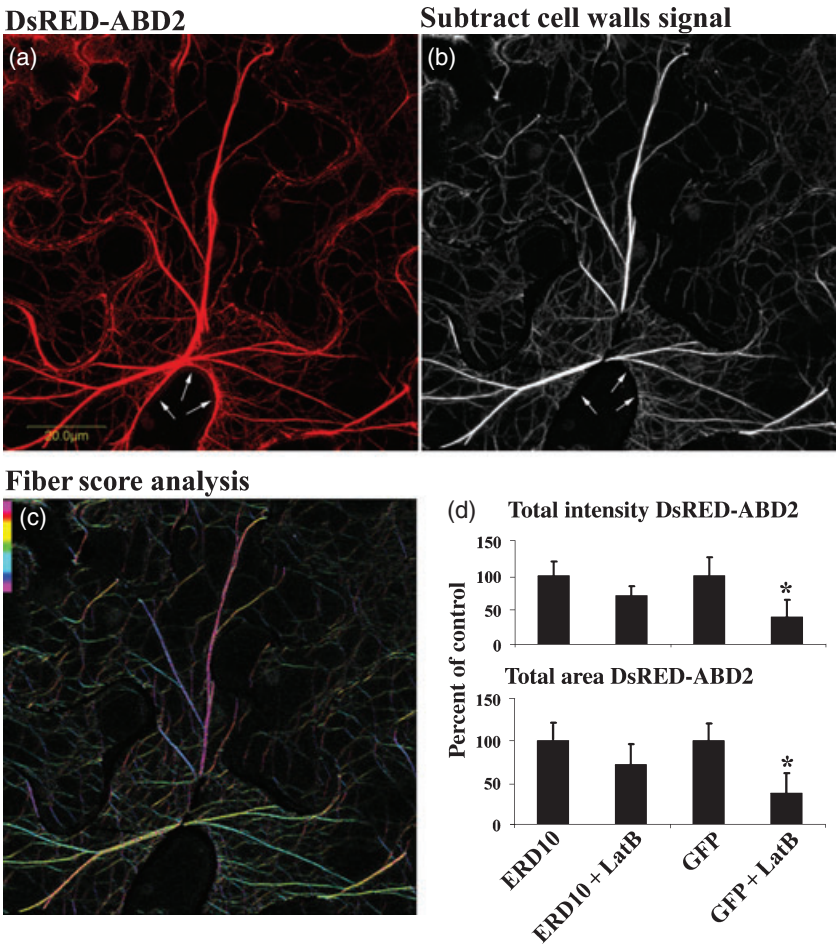

Figure 7. . Quantitative analysis of LatB-mediated disruption of actin filaments in either the presence or the absence of ERD10. Images of DsRED-ABD2-labeled actin filaments were analyzed by the FiberScore image analysis software (Lichtenstein *et al.*, 2003).
Before being subjected to analysis, fluorescence around the cell walls was subtracted from each field because of poor resolution of filaments in this vicinity (arrows). The values of total fluorescence associated with filaments and the total area of filaments were calculated for 10 microscopic fields of each treatment in three independent experiments. (a), original image; (b), image after cell-wall subtraction; (c), the image as interpreted by the computer (which gave the fibers colors according to angles: 0°, purple; 45°, blue; 90°, green; 135°, red; 180°, purple); (d), bar chart summarizing the data, asterisks show significant difference calculated by Student's *t*-test ($P < 0.005$). Values were divided by the average score for DsRED-ABD fluorescence in control untreated leaves in the presence of either ERD10 or GFP and multiplied by a hundred. Scale bar, 20 μm.

intensity and area of actin filaments remained after LatB treatment (Figure 7). The difference was statistically significant as tested by Student's *t*-test ($P < 0.005$; Figure 7,*).

Discussion

Several screens of GFP-fusion cDNA libraries expressed in plants and animal cells have been reported (for example, see Cutler *et al.*, 2000; Escobar *et al.*, 2003; Rolls *et al.*, 1999; Tian *et al.*, 2004). However, our system is unique in the fact that it combines a plant YFP-fusion library with expression in mammalian cell hosts serving as the screening system. We believe that our system is advantageous for the following reasons:

1 Optical limitations: adhesion to the cover-slide substrate, flattening and single-layer growth of adherent animal cells in tissue culture makes microscopy easier when compared with large, cell-wall encased and thick plant cells. High-resolution microscopy is dramatically limited by the short working distance of high-magnification high-numerical aperture objectives.
2 Signal-to-noise limitations: auto-fluorescence of the cell wall, phenols and chlorophyll is often very high in plant cells. In addition, the cytoplasm is a thin layer pressed between the vacuole and cell wall. The absorption and emission spectra of auto-fluorescence is very broad, leaving no 'clean' window in the visible range for specific labeling. The microscopy images suffer from both a very high background and a strong absorption of the specifically labeled fluorescence.
3 Cell biological limitations: transformation efficiency and rate of growth has been optimized for mammalian cell lines, ensuring that the number of individual infected cells screened will represent a full expression library. This is extremely important in this 'post genome' era when we design sophisticated functional genomic, high-throughput screens to look for new, low-abundance proteins that have so far escaped other 'conventional' and bioinformatic screens.
4 Automation of microscopy facilitates a comprehensive high-throughput screening.
5 Ref52 fibroblasts are large and flat cells with prominent stress fibers, thus serving as an optimal platform for detecting cytoskeletal components under the microscope.

Unlike other screens based on GFP-fused proteins in plants (Cutler *et al.*, 2000; Escobar *et al.*, 2003; Rolls *et al.*,

1999; Tian *et al.*, 2004), we were able to detect new plant YFP-cDNAs decorating actin fibers. Furthermore, for two isolated genes we confirm the ability to associate with the actin cytoskeleton by using independent methods.

Using this system we were able to find that the dehydrin ERD10 is associated with actin stress fibers in rat fibroblasts, binds directly to actin filaments *in vitro* and protects actin filaments from disruption by LatB in *N. benthamiana* leaves. It is notable that a second dehydrin family member, COR47, was also identified in the pilot library screen. We chose to focus further attention on just one of these related genes. In our hands, overexpressed ERD10 in *N. benthamiana* cells appeared to be predominantly cytoplasmic rather than cytoskeletal associated. Since it is a weak actin binding protein it is likely that many molecules remain unbound. Maize DHN was shown to be associated with a membrane-rich area surrounding lipids and protein bodies in scutellar parenchyma cells (Asghar *et al.*, 1994; Egerton-Warburton *et al.*, 1997). In wheat, an acidic DHN accumulated near the plasma membrane under cold stress (Danyluk *et al.*, 1998). Dehydrin-like protein was observed in association with plasmodesmata of cold-acclimated vascular cambium cells of red-osier dogwood (*Cornus sericea* L.; Karlson *et al.*, 2003). In addition, maize DHN1 can bind lipid vesicles that contain acidic phospholipids *in vitro* (Koag *et al.*, 2003). Integrating these data and our findings suggests that ERD10 may participate in the cross-talk between the actin cytoskeleton and membranous organelles in plant cells. Although their physiological role is not well understood, dehydrins have been proposed to function as membrane stabilizers during freeze-induced dehydration (Danyluk *et al.*, 1998), to possess either cryoprotective (Bravo *et al.*, 2003) or anti-freeze activity (Wisniewski *et al.*, 1999), to function as possible osmo-regulators (Nylander *et al.*, 2001), to improve enzyme activity (Rinne *et al.*, 1999) or to act as radical scavengers (Hara *et al.*, 2003). Recently, it was shown that DHN/DHN-like proteins can bind calcium in a phosphorylation-dependent manner (Alsheikh *et al.*, 2003; Heyen *et al.*, 2002), suggesting that DHNs might act as either calcium buffers or calcium-dependent chaperones like calreticulin and calnexin. Simultaneous overexpression of two dehydrin genes enhanced tolerance to freezing stress in Arabidopsis (Puhakainen *et al.*, 2004). Interestingly, bioinformatic analysis of dehydrins revealed a potential for their association with the cytoskeleton (Wise, 2003). We show here that ERD10 can bind the actin cytoskeleton *in vitro* and protect it from disruption mediated by dilution *in vitro* and by LatB *in vivo*. There are multiple indications that the actin cytoskeleton is involved in abiotic stress signaling in plant cells. Cold induction of specific genes and calcium influx was inhibited by jasplakinolide (JP), an actin filament stabilizing agent, but induced at 25°C by the actin depolymerizing compound cytochalasin D (CD; Orvar *et al.*, 2000; Sangwan *et al.*, 2001, 2002). Salt-induced mitogen-activated protein kinase (MAPK), SIMK, was activated by both JP and LatB and localized to thick actin cables in root hairs of Medicago following JP treatment (Samaj *et al.*, 2002). Trafficking of early endosomes is compromised in actin mutants (Grebe *et al.*, 2003) and pharmacological studies using LatB and CD reveal that the actin cytoskeleton is important for endocytosis (Baluska *et al.*, 2002, 2004; Samaj *et al.*, 2004, 2005), which is crucial in stress responses (Bolte *et al.*, 2000; Leyman *et al.*, 1999; Mazel *et al.*, 2004; Ueda *et al.*, 2001; Zerial and McBride, 2001). In addition, ADF is induced in plants by different stress signals (Buchanan *et al.*, 2005; Ouellet *et al.*, 2001; Yan *et al.*, 2005), as is fimbrin (Cruz-Ortega *et al.*, 1997). Thus, by binding to actin filaments and protecting them from depolymerization, ERD10 may be involved in an additional level of regulation of actin dynamics during stress conditions.

The second putative cytoskeletal-associated protein identified in our small-scale library screening, TCH2, a calmodulin-like protein, was found to interact with the four IQ domains of plant myosin VIII (ATM1) in a calcium-dependent manner. Of note, and consistent with previous findings (Yokota *et al.*, 1999), calcium was inhibitory to TCH2–IQ interaction. The distribution of myosin VIII was characterized in maize roots using immunofluorescent studies with specific antibodies (Baluska *et al.*, 2001; Reichelt *et al.*, 1999). It was shown that myosin VIII distributes differently in different cells. In root-cap cells, it was spread diffusely throughout the cytoplasm. In the distal part of the apical meristem, the anti-myosin VIII antibodies stained fine spots representing plasmodesmata. In the distal part of the transition zone and in the distal part of the elongation region, these spots were more prominent where the signal corresponds to plasmodesmata clustered into pit fields. When viewing cross sections of root apices, myosin VIII accumulated at cell-to-cell contacts, whereas cell periphery domains facing intercellular spaces were depleted of myosin VIII. In the post-mitotic cells of the outer cortex, myosin VIII showed a faint signal and it did not localize to cellular peripheries. Of significant note and importance to the current study, myosin VIII does not localize along actin filaments in plants (Baluska *et al.*, 2001; Reichelt *et al.*, 1999). Thus, we might not expect similar cellular localization in mammalian cells and plant cells in this case. When YFP-TCH2 was transiently expressed in *N. benthamiana* leaves it was distributed diffusely in the cytoplasm, probably as a result of high levels of overexpression (not shown).

Taken together the current findings suggest that our system has an enormous potential for functional screening and revealing new plant cytoskeletal proteins, which could not be identified by the screening of GFP-fused libraries in plants, by bioinformatics or by cross-reaction of antibodies.

Experimental procedures

The automated microscope

A microscope system was developed that included a computer-controlled stage for multi-well plate scanning, fast laser auto-focusing for high magnification imaging, extremely sensitive back-illuminated digital CCD camera (quantum efficiency is >95% throughout the visible and IR wavelengths) and modular controlling software for fully automated operation. The system acquired 20 Gb of image data per day, and via a client-server link saved and analyzed the data practically on-line (Liron *et al.*, 2006). Currently, the images are collected automatically but inspected and sorted manually.

Constructing the library

A cDNA library was prepared from 2-week-old *Arabidopsis thaliana* type Columbia seedlings (The Arabidopsis Biological Resource Centre (ABRC) Ohio State University, OH, USA). The library was constructed using the Smart cDNA library construction kit (Cat No. K1051-1; Clontech, Palo Alto, CA, USA). The expression vector used for fusion to YFP is the Clontech retroviral vector pLPCX that was modified as follows: a cDNA of the improved, higher fluorescent Venus version of YFP (Nagai *et al.*, 2002), without its ATG was inserted between the *Not*I and *Cla*I of the pLPCX multiple cloning site. A *Bam*HI site and a linker of Ser-Gly-Thr-Gly-Ser in three reading frames were added upstream to the YFP (Figure 1). The full-length Arabidopsis cDNAs were first digested with *Sfi*I and then partially digested with *Sau*3A, which is a four-cutter enzyme compatible with *Bam*HI. The cDNA fragments were ligated between *Sfi*IA and *Bam*HI (Figure 1).

Mammalian tissue culture, infections and transfections

Ref52 and 293T cells were cultured in Dulbecco's modified Eagle's medium (DMEM) supplemented with 10% fetal calf serum, in a 37°C/5% CO_2 incubator. For infection, 293T cells were transfected with 10 μg of library DNA and 10 μg of helper virus using the Ca-phosphate method in the presence of 25 μM chloroquine (C-6628; Sigma, Rehovot, Israel). After 2 days the virions were collected from the medium, filtered through a 0.45-μm nitrocellulose filter and added to the Ref52 culture with 8 μg ml^{-1} polybrene (H-9268; Sigma). The latter step was repeated three times. Ref 52 cells were fixed with 3% paraformaldehyde in PBS 48 h after infection and examined by the microscope. Transfection into Ref52 cells was carried out with TransIT reagent (Mirus, Madison, WI, USA) using the manufacturer's instructions.

The pilot screen

Bacterial colonies containing the Arabidopsis cDNA clones were individually collected into sixty 96-well plates (5–10 clones per well). DNA was prepared from two pools of 2500 clones (five 96-well plates). The pooled DNA was infected into rat fibroblasts, screened with the microscope and scored for potential clones that showed interesting sub-cellular localization patterns. The fibroblast cells were infected in 384-well plates (#781091; greiner bio-one, Frickenhausen, Germany). Each well was seeded with 300–500 cells that were infected, cultured for 2 days and screened. Each pool yielding cytoskeleton localizing clones was sub-divided into smaller pools of 500 clones (stored in one 96-well plate). From the positive 96-well plates we prepared eight pools from the rows and 12 pools from the columns. These were screened and positive clones were localized in the wells at the intersection of a positive row and column.

Fluorescent staining, microscopy and image analysis

Single clones localizing to actin stress fibers were isolated from the wells and purified DNA was re-transfected into Ref52 cells cultured on a cover slip. The verification of their localization was carried out by double labeling with specific markers such as coumarine-phalloidin (P-2495; Sigma) for actin filaments and anti-vinculin antibody (H Vin), a marker for focal contacts, and a fluorescent secondary antibody conjugated to Cy3 (115–165-072; Jackson ImmunoResearch, West Grove, PA, USA). Images were acquired by an IX81 Olympus microscope (Olympus, Hamburg, Germany) equipped with an Orca C4742-80-12AG CCD camera (Hamamatsu, Hamamatsu-City, Japan) and each fluorophore was colored artificially. *N. benthamiana* leaves were inspected by a confocal Olympus IX81 microscope equipped with an FV500 scanner (Olympus). GFP was detected by a 488-nm excitation filter and BA505–525 and red fluorescent protein was detected by a 543-nm excitation filter and BA 560 filter (Olympus). Image analysis was performed using the FiberScore software, available under priism (Lichtenstein *et al.*, 2003)(http://msg.ucsf.edu/IVE/).

RT-PCR and plasmids

Full-length cDNAs for Arabidopsis ERD10 (accession number NM_180616, AT1G20450) and TCH2 (accession number NM_123136, AT5G37770) were isolated from Arabidopsis RNA using RT-PCR and the following primers: an ERD10 forward primer containing an *Eco*RI site, 5′-CGGAATTCATGGCAGAAGAGTACAAGAACACCGTTCCA-3′ and a reverse primer with *Bam*HI site 5′-CGGGATCCATCAGACACTTTTTCTTTCTTCTCTTCCTC-3′; a TCH2 forward primer containing *Hind*III, 5′-CCCAAGCTTATGTCATCGAAGAACGGAGTT-3′ and a reverse primer containing *Bam*HI 5′-CGGGATCCAGCACCACCACCATTACTCAT-3′. The PCR products were ligated upstream to YFP in one of the vectors prepared for the library according to the reading frame. The fluorescent chimera was transferred into the plant expression vector pART7 containing the 35S promoter and as a full expression cassette into the binary vector pART27. For GST fusion protein expression, ERD10 was amplified using the following primers 5′-CGGGATCCATGGCAGAAGAGTACAAGAACACCGTTCCA-3′ and 5′-CGGAATTCTTAATCAGACACTTTTTCTTTCTTCTCTTCCTC-3′ and ligated into the pGEX-KG plasmid (Guan and Dixon, 1991) between *Bam*HI and *Eco*RI. The 4XIQ domain of myosin VIII (ATM1) from nucleotide 2651–2929 was isolated by PCR from a cDNA clone kindly provided by Dieter Volkmann (University of Bonn, Bonn, Germany) and fused to GST between *Bam*HI and *Eco*RI using the following primers: 5′-CGGGATCCCTCCACGGCATTTTACGT-3′ and 5′-CGGAATTCTTACCCTGAACATCTTCTAAC-3′. ERD10 was fused to the C-terminus of GFP, after a link comprising ten alanine residues with the restriction enzymes *Kpn*I and *Cla*I, into the vector pART7 and under the promoter 35S. The whole expression cassette was ligated using *Not*I sites into the binary vector pART27. The plasmid pCB DsRED-ABD2 was kindly provided by Jozef Samaj (University of Bonn) (Voigt *et al.*, 2005). The cDNA of TCH1 was isolated by RT-PCR using the following primers: 5′-CGGAATTCATGGCAGATCAGCTCACCGATGAT-3′ and 5′-CGGGATCCCTTTGCCATCATAACTTTGACAAA-3′ and fused to YFP in the pLPCX vector.

Actin purification

Actin was purified from rabbit skeletal muscle acetone powder (Spudich and Watt, 1971), and monomeric Ca-ATP-actin was purified by Sephacryl S-300 chromatography (Pollard, 1984) in Buffer G (5 mM Tris-HCl, pH 8, 0.2 mM ATP, 0.1 mM $CaCl_2$, 0.5 mM DTT, 0.1 mM azide). Actin was labeled on Cys-374 with pyrene iodoacetamide (Pollard, 1984).

Critical concentration determination at steady state

The critical concentration (C_c) for actin polymerization was determined as described by Brenner and Korn (1983). Increasing concentrations of actin (5% pyrene-labeled) were polymerized in 1× KMEI (50 mM KCl, 1 mM $MgCl_2$,1 mM EGTA and 10 mM imidazole-HCl, pH 7.0) in either the absence or the presence of 2 μM ERD10 or 1 μM HPRO1 (human profilin I) for 16 h at 25° C in the dark. Human plasma gelsolin at 1:200 stoichiometry was used to cap the barbed ends of actin filaments. Fluorescence measurements were performed at room temperature using a spectrofluorometer (Quantamaster 4SE; Photon Technology International, South Brunswick, NJ, USA) with excitation set at 365 nm and emission detected at 407 nm. Linear best fit of the data, plotted as arbitrary fluorescence units versus actin concentration, was used to determine the intercept with the *x*-axis (C_c).

Kinetic studies of actin polymerization and depolymerization

Kinetic analysis of actin assembly and disassembly was monitored by changes in pyrene fluorescence according to assays described previously (Huang *et al.*, 2005). The polymerization of monomeric actin in the presence of various concentrations of ERD10 was measured over time. Actin monomers (2 μM, 5% pyrene-labeled) were polymerized with the addition of 0.1 volume of 10× KMEI and the change in fluorescence was followed for 30 min. To document effects on actin depolymerization, pyrene-actin filaments (5 μM; 100% labeled) were assembled and then pre-incubated for 5 min in either the presence or the absence of various quantities of actin-binding proteins (ERD10 and FIMBRIN1). Depolymerization was monitored by fluorimetry following dilution of the sample by 25-fold with buffer G.

GST pull-down assay

Plasmids with either GST-IQ or GST alone were transformed into BL21 *E. coli* cells and expression was induced with 0.4 mM isopropyl-β-D-thiogalactopyranoside (IPTG) for 4 h at 37°C. Bacterial cell pellets were re-suspended in Perp. Buffer (100 mM NaCl, 100 mM Tris HCl pH 8, 50 mM EDTA, 2% Triton X-100, 2 mM DTT) supplemented with a protease inhibitors cocktail (P 8465; Sigma) and 10 mg ml^{-1} lysozyme (L-7651; Sigma) and was incubated 30 min on ice. Debris was precipitated at 17 000 ***g*** at 4°C for 10 min and the extracts were incubated with 20 μl of glutathione-agarose beads (G-4510; Sigma) for 1 h at room temperature. The glutathione beads were washed with the same buffer and incubated with cell lysate of 293T expressing TCH2 or TCH1-YFP. The 293T cell culture was transfected with either TCH2-YFP or TCH1-YFP and 48 h later harvested in a buffer containing 40 mM HEPES, pH 7.5, 100 mM NaCl, 5 mM $MgCl_2$, 4% glycerol, 0.5% Triton X-100, 5 mM DTT, 1 mM phenylmethylsulfonyl fluoride (PMSF) and either 5 mM EGTA or 5 mM $CaCl_2$. After 2 h of incubation at 4°C the beads were washed six times with buffer containing 20 mM Tris, pH 8, 150 mM NaCl, 0.5% NP40 and either 5 mM EGTA or 5 mM $CaCl_2$, respectively. The beads were boiled in sample buffer and bound proteins were separated on an SDS-PAGE gel. TCH2 TCH1-YFP were detected with anti-GFP antibody (1 814 460; Roche, Basel, Switzerland).

Transient expression in N. benthamiana *leaves*

N. benthamiana plants were grown in peat in a greenhouse at 25°C with optimum light for 16 h. The fluorescent chimeras were expressed using Agrobacterium infiltration. Briefly: bacteria of *Agrobacterium tumefaciens* strain GVE3101 were transformed with the plasmids and grown at 28°C for 48 h. The culture was precipitated and dissolved to $OD_{600} = 0.5$ in the following buffer: 50 mM 2-(*N*-morpholine)-ethanesulphonic acid (MES), pH 5.6, 0.5% glucose, 2 mM $NaPO_4$ and 100 μM acetosyringone (D13440-6; Sigma Aldrich). Leaves of 3-week-old *N. benthamiana* plants were infiltrated with the bacterial culture using a syringe. To see GFP and DsRED together, bacteria were infiltrated at the ratio 1:2 GFP/DsRED. Expression of the fluorescent chimeras in the leaf cells was detectable after 24 h, peaking at 48 h and still observable after 5 days. Leaf disks from the infiltrated leaves were treated with 25μM Latrunculin B (L-5288; Sigma) in PBS for 5 h prior to microscopy inspection.

Acknowledgements

This research was supported by Research Grant No. IS-3460-03 from BARD, the United States-Israel Binational Agricultural Research and Development Fund for ES, CS and ZK, and from the Israeli Science Foundation (ISF) for ES and ZK. The authors thank J-K. Min and S. Lu (Purdue) for providing some batches of rabbit muscle actin, F. Chaudhry (Purdue) for pyrene-labeled actin, and B. Zimerman (Volcani) for purifying recombinant ERD10 and TCH2.

Supplementary Material

The following supplementary material is available for this article online:

Figure S1. The scanning path of the automatic microscope.

Figure S2. A list of the genes isolated.

This material is available as part of the online article from http://www.blackwell-synergy.com.

References

Alsheikh, M.K., Heyen, B.J. and Randall, S.K. (2003) Ion binding properties of the dehydrin ERD14 are dependent upon phosphorylation. *J. Biol. Chem.* **278**, 40882–40889.

Asghar, R., Fenton, R.D., DeMason, D.A. and Close, T.J. (1994) Nuclear and cytoplasmic localization of maize embryo and aleurone dehydrin. *Protoplasma*, **177**, 87–94.

Assaad, F.F. (2001) Of weeds and men: what genomes teach us about plant cell biology. *Curr. Opin. Plant Biol.* **4**, 478–487.

Bahler, M. and Rhoads, A. (2002) Calmodulin signaling via the IQ motif. *FEBS Lett.* **513**, 107–113.

Baluska, F., Cvrckova, F., Kendrick-Jones, J. and Volkmann, D. (2001) Sink plasmodesmata as gateways for phloem unloading. Myosin VIII and calreticulin as molecular determinants of sink strength? *Plant Physiol.* **126**, 39–46.

Baluska, F., Hlavacka, A., Samaj, J., Palme, K., Robinson, D.G., Matoh, T., McCurdy, D.W., Menzel, D. and Volkmann, D. (2002)

F-actin-dependent endocytosis of cell wall pectins in meristematic root cells. Insights from brefeldin a-induced compartments. *Plant Physiol.* **130**, 422–431.

Baluska, F., Samaj, J., Hlavacka, A., Kendrick-Jones, J. and Volkmann, D. (2004) Actin-dependent fluid-phase endocytosis in inner cortex cells of maize root apices. *J. Exp. Bot.* **55**, 463–473.

Bolte, S., Schiene, K. and Dietz, K.J. (2000) Characterization of a small GTP-binding protein of the rab 5 family in Mesembryanthemum crystallinum with increased level of expression during early salt stress. *Plant Mol. Biol.* **42**, 923–936.

Braam, J. and Davis, R.W. (1990) Rain-, wind-, and touch-induced expression of calmodulin and calmodulin-related genes in Arabidopsis. *Cell*, **60**, 357–364.

Bravo, L.A., Gallardo, J., Navarrete, A., Olave, N., Martinez, J., Alberdi, M., Close, T.J. and Corcuera, L.J. (2003) Cryoprotective activity of a cold-induced dehydrin purified from barley. *Physiol. Plant*, **1128**, 262–269.

Brenner, S.L. and Korn, E.D. (1983) On the mechanism of actin monomer-polymer subunit exchange at steady state. *J. Biol. Chem.* **258**, 5013–5020.

Buchanan, C.D., Lim, S., Salzman, R.A. *et al.* (2005) Sorghum bicolor's transcriptome response to dehydration, high salinity and ABA. *Plant Mol. Biol.* **58**, 699–720.

Carlier, M.F., Laurent, V., Santolini, J., Melki, R., Didry, D., Xia, G.X., Hong, Y., Chua, N.H. and Pantaloni, D. (1997) Actin depolymerizing factor (ADF/cofilin) enhances the rate of filament turnover: implication in actin-based motility. *J. Cell Biol.* **136**, 1307–1322.

Chan, J., Jensen, C.G., Jensen, L.C., Bush, M. and Lloyd, C.W. (1999) The 65-kDa carrot microtubule-associated protein forms regularly arranged filamentous cross-bridges between microtubules. *Proc. Natl Acad. Sci. USA*, **96**, 14931–14936.

Cruz-Ortega, R., Cushman, J.C. and Ownby, J.D. (1997) cDNA clones encoding 1,3-beta-glucanase and a fimbrin-like cytoskeletal protein are induced by Al toxicity in wheat roots. *Plant Physiol.* **114**, 1453–1460.

Cutler, S.R., Ehrhardt, D.W., Griffitts, J.S. and Somerville, C.R. (2000) Random GFP:cDNA fusions enable visualization of subcellular structures in cells of Arabidopsis at a high frequency. *Proc. Natl Acad. Sci. USA*, **97**, 3718–3723.

Cyert, M.S. (2001) Genetic analysis of calmodulin and its targets in *Saccharomyces cerevisiae*. *Annu. Rev. Genet.* **35**, 647–672.

Danyluk, J., Perron, A., Houde, M., Limin, A., Fowler, B., Benhamou, N. and Sarhan, F. (1998) Accumulation of an acidic dehydrin in the vicinity of the plasma membrane during cold acclimation of wheat. *Plant Cell*, **10**, 623–638.

Deeks, M.J. and Hussey, P.J. (2003) Arp2/3 and 'the shape of things to come'. *Curr. Opin. Plant Biol.* **6**, 561–567.

Deeks, M.J., Hussey, P.J. and Davies, B. (2002) Formins: intermediates in signal-transduction cascades that affect cytoskeletal reorganization. *Trends Plant Sci.* **7**, 492–498.

Dong, C.H., Kost, B., Xia, G. and Chua, N.H. (2001) Molecular identification and characterization of the Arabidopsis AtADF1, AtADF5 and AtADF6 genes. *Plant Mol. Biol.* **45**, 517–527.

Drøbak, B.K., Franklin-Tong, V.E. and Staiger, C.J. (2004) Tansley review: the role of the actin cytoskeleton in plant cell signaling. *New Phytol.* **163**, 13–30.

Egerton-Warburton, L.M., Balsamo, R. and Close, T.J. (1997) Temporal accumulation and ultrastructural localization of dehydrins in *Zea maize* L. *Physiol. Plant* **101**, 545–555.

Escobar, N.M., Haupt, S., Thow, G., Boevink, P., Chapman, S. and Oparka, K. (2003) High-throughput viral expression of cDNA-green fluorescent protein fusions reveals novel subcellular addresses and identifies unique proteins that interact with plasmodesmata. *Plant Cell*, **15**, 1507–1523.

Fu, Y., Gu, Y., Zheng, Z., Wasteneys, G. and Yang, Z. (2005) Arabidopsis interdigitating cell growth requires two antagonistic pathways with opposing action on cell morphogenesis. *Cell*, **120**, 687–700.

Grebe, M., Xu, J., Mobius, W., Ueda, T., Nakano, A., Geuze, H.J., Rook, M.B. and Scheres, B. (2003) Arabidopsis sterol endocytosis involves actin-mediated trafficking via ARA6-positive early endosomes. *Curr. Biol.* **13**, 1378–1387.

Gu, Y., Fu, Y., Dowd, P., Li, S., Vernoud, V., Gilroy, S. and Yang, Z. (2005) A Rho family GTPase controls actin dynamics and tip growth via two counteracting downstream pathways in pollen tubes. *J. Cell Biol.* **169**, 127–138.

Guan, K.L. and Dixon, J.E. (1991) Eukaryotic proteins expressed in *Escherichia coli*: an improved thrombin cleavage and purification procedure of fusion proteins with glutathione S-transferase. *Anal. Biochem.* **192**, 262–267.

Gunning, B.E.S. and Hardham, A.R. (1982) Microtubules. *Annu. Rev. Plant Physiol* **33**, 651–698.

Hara, M., Terashima, S., Fukaya, T. and Kuboi, T. (2003) Enhancement of cold tolerance and inhibition of lipid peroxidation by citrus dehydrin in transgenic tobacco. *Planta*, **217**, 290–298.

Heyen, B.J., Alsheikh, M.K., Smith, E.A., Torvik, C.F., Seals, D.F. and Randall, S.K. (2002) The calcium-binding activity of a vacuole-associated, dehydrin-like protein is regulated by phosphorylation. *Plant Physiol.* **130**, 675–687.

Higashi-Fujime, S., Ishikawa, R., Iwasawa, H., Kagami, O., Kurimoto, E., Kohama, K. and Hozumi, T. (1995) The fastest actin-based motor protein from the green algae, Chara, and its distinct mode of interaction with actin. *FEBS Lett.* **375**, 151–154.

Huang, S., Blanchoin, L., Chaudhry, F., Franklin-Tong, V.E. and Staiger, C.J. (2004) A gelsolin-like protein from *Papaver rhoeas* pollen (PrABP80) stimulates calcium-regulated severing and depolymerization of actin filaments. *J. Biol. Chem.* **279**, 23364–23375.

Huang, S., Robinson, R.C., Gao, L.Y., Matsumoto, T., Brunet, A., Blanchoin, L. and Staiger, C.J. (2005) Arabidopsis VILLIN1 generates actin filament cables that are resistant to depolymerization. *Plant Cell*, **17**, 486–501.

Huang, S., Gao, L., Blanchoin, L. and Staiger, C.J. (2006) Heterodimeric capping protein from Arabidopsis is regulated by phosphatidic Acid. *Mol. Biol. Cell.* **17**, 1946–1958.

Hussey, P.J., Allwood, E.G. and Smertenko, A.P. (2002) Actin-binding proteins in the Arabidopsis genome database: properties of functionally distinct plant actin-depolymerizing factors/cofilins. *Philos. Trans. R. Soc. Lond. B Biol. Sci.* **357**, 791–798.

Karlson, D.T., Fujino, T., Kimura, S., Baba, K., Itoh, T. and Ashworth, E.N. (2003) Novel plasmodesmata association of dehydrin-like proteins in cold- acclimated Red-osier dogwood (Cornus sericea). *Tree Physiol.* **23**, 759–767.

Kinkema, M. and Schiefelbein, J. (1994) A myosin from a higher plant has structural similarities to class V myosins. *J. Mol. Biol.* **239**, 591–597.

Kiyosue, T., Yamaguchi-Shinozaki, K. and Shinozaki, K. (1994) Characterization of two cDNAs (ERD10 and ERD14) corresponding to genes that respond rapidly to dehydration stress in *Arabidopsis thaliana*. *Plant Cell Physiol.* **35**, 225–231.

Klahre, U., Friederich, E., Kost, B., Louvard, D. and Chua, N.H. (2000) Villin-like actin-binding proteins are expressed ubiquitously in Arabidopsis. *Plant Physiol.* **122**, 35–48.

Koag, M.C., Fenton, R.D., Wilkens, S. and Close, T.J. (2003) The binding of maize DHN1 to lipid vesicles. Gain of structure and lipid specificity. *Plant Physiol.* **131**, 309–316.

Kovar, D.R., Staiger, C.J., Weaver, E.A. and McCurdy, D.W. (2000) AtFim1 is an actin filament crosslinking protein from *Arabidopsis thaliana*. *Plant J.* **24**, 625–636.

Kreis, T. and Vale, R. (1999) *Guidebook to the cytoskeleton and motor proteins*, 2nd edn. New York: Oxford University Press.

Leyman, B., Geelen, D., Quintero, F.J. and Blatt, M.R. (1999) A tobacco syntaxin with a role in hormonal control of guard cell ion channels. *Science*, **283**, 537–540.

Lichtenstein, N., Geiger, B. and Kam, Z. (2003) Quantitative analysis of cytoskeletal organization by digital fluorescent microscopy. *Cytometry*, **54A**, 8–18.

Liron, Y., Paran, Y., Zatorsky, N.G., Geiger, B. and Kam, Z. (2006) Laser autofocusing system for high-resolution cell biological imaging. *J. Microsc.* **221**, 145–151.

Mathur, J. (2005) The ARP2/3 complex: giving plant cells a leading edge. *Bioessays*, **27**, 377–387.

Mazel, A., Leshem, Y., Tiwari, B.S. and Levine, A. (2004) Induction of salt and osmotic stress tolerance by overexpression of an intracellular vesicle trafficking protein AtRab7 (AtRabG3e). *Plant Physiol.* **134**, 118–128.

McCormack, E., Tsai, Y.C. and Braam, J. (2005) Handling calcium signaling: Arabidopsis CaMs and CMLs. *Trends Plant Sci.* **10**, 383–389.

McCurdy, D.W. and Kim, M. (1998) Molecular cloning of a novel fimbrin-like cDNA from *Arabidopsis thaliana*. *Plant Mol. Biol.* **36**, 23–31.

McKinney, E.C., Kandasamy, M.K. and Meagher, R.B. (2002) Arabidopsis contains ancient classes of differentially expressed actin-related protein genes. *Plant Physiol.* **128**, 997–1007.

Meagher, R.B. and Williamson, R.E. (1994) The plant cytoskeleton. In *Arabidopsis*. (Meyerowitz, E. and Somerville, C., eds). Cold Spring Harbor, NY: Cold Spring Harbor Press, pp. 1049–1084.

Meagher, R.B., McKinney, E.C. and Kandasamy, M.K. (1999a) Isovariant dynamics expand and buffer the responses of complex systems: the diverse plant actin gene family. *Plant Cell*, **11**, 995–1006.

Meagher, R.B., McKinney, E.C. and Vitale, A.V. (1999b) The evolution of new structures: clues from plant cytoskeletal genes. *Trends Genet.* **15**, 278–284.

Michelot, A., Guerin, C., Huang, S., Ingouff, M., Richard, S., Rodiuc, N., Staiger, C.J. and Blanchoin, L. (2005) The Formin Homology 1 domain modulates the actin nucleation and bundling activity of Arabidopsis FORMIN1. *Plant Cell*, **17**, 2296–2313.

Moller-Jensen, J. and Lowe, J. (2005) Increasing complexity of the bacterial cytoskeleton. *Curr. Opin. Cell Biol.* **17**, 75–81.

Nagai, T., Ibata, K., Park, E.S., Kubota, M., Mikoshiba, K. and Miyawaki, A. (2002) A variant of yellow fluorescent protein with fast and efficient maturation for cell-biological applications. *Nat. Biotechnol.* **20**, 87–90.

Nylander, M., Svensson, J., Palva, E.T. and Welin, B.V. (2001) Stress-induced accumulation and tissue-specific localization of dehydrins in *Arabidopsis thaliana*. *Plant Mol. Biol.* **45**, 263–279.

Orvar, B.L., Sangwan, V., Omann, F. and Dhindsa, R.S. (2000) Early steps in cold sensing by plant cells: the role of actin cytoskeleton and membrane fluidity. *Plant J.* **23**, 785–794.

Ouellet, F., Carpentier, E., Cope, M.J., Monroy, A.F. and Sarhan, F. (2001) Regulation of a wheat actin-depolymerizing factor during cold acclimation. *Plant Physiol.* **125**, 360–368.

Pollard, T.D. (1984) Polymerization of ADP-actin. *J. Cell Biol.* **99**, 769–777.

Pollard, T.D. (2001) Genomics, the cytoskeleton and motility. *Nature*, **409**, 842–843.

Puhakainen, T., Hess, M.W., Makela, P., Svensson, J., Heino, P. and Palva, E.T. (2004) Overexpression of multiple dehydrin genes enhances tolerance to freezing stress in Arabidopsis. *Plant Mol. Biol.* **54**, 743–753.

Reichelt, S., Knight, A.E., Hodge, T.P., Baluska, F., Samaj, J., Volkmann, D. and Kendrick-Jones, J. (1999) Characterization of the unconventional myosin VIII in plant cells and its localization at the post-cytokinetic cell wall. *Plant J.* **19**, 555–567.

Reinhard, M., Giehl, K., Abel, K., Haffner, C., Jarchau, T., Hoppe, V., Jockusch, B.M. and Walter, U. (1995) The proline-rich focal adhesion and microfilament protein VASP is a ligand for profilins. *EMBO J.* **14**, 1583–1589.

Rinne, P.L., Kaikuranta, P.L., van der Plas, L.H. and van der Schoot, C. (1999) Dehydrins in cold-acclimated apices of birch (Betula pubescens ehrh.): production, localization and potential role in rescuing enzyme function during dehydration. *Planta*, **209**, 377–388.

Rolls, M.M., Stein, P.A., Taylor, S.S., Ha, E., McKeon, F. and Rapoport, T.A. (1999) A visual screen of a GFP-fusion library identifies a new type of nuclear envelope membrane protein. *J. Cell Biol.* **146**, 29–44.

Rothkegel, M., Mayboroda, O., Rohde, M., Wucherpfennig, C., Valenta, R. and Jockusch, B.M. (1996) Plant and animal profilins are functionally equivalent and stabilize microfilaments in living animal cells. *J. Cell Sci.* **109**, 83–90.

Samaj, J., Ovecka, M., Hlavacka, A. *et al.* (2002) Involvement of the mitogen-activated protein kinase SIMK in regulation of root hair tip growth. *EMBO J.* **21**, 3296–3306.

Samaj, J., Baluska, F., Voigt, B., Schlicht, M., Volkmann, D. and Menzel, D. (2004) Endocytosis, actin cytoskeleton, and signaling. *Plant Physiol.* **135**, 1150–1161.

Samaj, J., Read, N.D., Volkmann, D., Menzel, D. and Baluska, F. (2005) The endocytic network in plants. *Trends Cell Biol.* **15**, 425–433.

Sangwan, V., Foulds, I., Singh, J. and Dhindsa, R.S. (2001) Cold-activation of *Brassica napus* BN115 promoter is mediated by structural changes in membranes and cytoskeleton, and requires Ca2+ influx. *Plant J.* **27**, 1–12.

Sangwan, V., Orvar, B.L., Beyerly, J., Hirt, H. and Dhindsa, R.S. (2002) Opposite changes in membrane fluidity mimic cold and heat stress activation of distinct plant MAP kinase pathways. *Plant J.* **31**, 629–638.

Spudich, J.A. and Watt, S. (1971) The regulation of rabbit skeletal muscle contraction. I. Biochemical studies of the interaction of the tropomyosin–troponin complex with actin and the proteolytic fragments of myosin. *J. Biol. Chem.* **246**, 4866–4871.

Staiger, C.J. and Hussey, P.J. (2004) Actin and actin-modulating proteins. In *The Plant Cytoskeleton in Cell Differentiation and Development*. (Hussey, P.J., eds). UK: Blackwell Publishers, pp. 32–80.

Szymanski, D.B. (2005) Breaking the WAVE complex: the point of Arabidopsis trichomes. *Curr. Opin. Plant Biol.* **8**, 103–112.

Thorn, K.S., Christensen, H.E., Shigeta, R., Huddler, D., Shalaby, L., Lindberg, U., Chua, N.H. and Schutt, C.E. (1997) The crystal structure of a major allergen from plants. *Structure*, **5**, 19–32.

Tian, G.W., Mohanty, A., Chary, S.N. *et al.* (2004) High-throughput fluorescent tagging of full-length Arabidopsis gene products in planta. *Plant Physiol.* **135**, 25–38.

Ueda, T., Yamaguchi, M., Uchimiya, H. and Nakano, A. (2001) Ara6, a plant-unique novel type Rab GTPase, functions in the endocytic pathway of *Arabidopsis thaliana*. *EMBO J.* **20**, 4730–4741.

Vesk, P.A., Vesk, M. and Gunning, B.E.S. (1996) Field emission scanning electron microscopy of microtubule array in higher plant cells. *Protoplasma*, **195**, 168–182.

Vidali, L., Yokota, E., Cheung, A.Y., Shimmen, T. and Hepler, P.K. (1999) The 135 kDa actin-bundling protein from *Lilium longiflorum* pollen is the plant homologue of villin. *Protoplasma*, **209**, 283–291.

Voigt, B., Timmers, A.C., Samaj, J., Muller, J., Baluska, F. and Menzel, D. (2005) GFP-FABD2 fusion construct allows in vivo visualization of the dynamic actin cytoskeleton in all cells of Arabidopsis seedlings. *Eur. J. Cell Biol.* **84**, 595–608.

Wise, M.J. (2003) LEAping to conclusions: a computational reanalysis of late embryogenesis abundant proteins and their possible roles. *BMC Bioinformatics*, **4**, 52.

Wisniewski, M., Webb, R., Balsamo, R., Close, T.J., Yu, X.M. and Griffith, M. (1999) Purification, immunolocalization, cryoprotective, and antifreeze activity of PCA60: a dehydrin from peach *(Prunus persica). Physiol. Plant*, **105**, 600–608.

Yan, S., Tang, Z., Su, W. and Sun, W. (2005) Proteomic analysis of salt stress-responsive proteins in rice root. *Proteomics*, **5**, 235–244.

Yokota, E., Muto, S. and Shimmen, T. (1999) Inhibitory regulation of higher-plant myosin by Ca2+ ions. *Plant Physiol.* **119**, 231–240.

Zerial, M. and McBride, H. (2001) Rab proteins as membrane organizers. *Nat. Rev. Mol. Cell Biol.* **2**, 107–117.

